

A Comparison of Methods for the Stochastic Simulation of Rock Fractures

Peter A. Dowd · Chaoshui Xu · Kanti V. Mardia ·
Robert J. Fowell

Received: 13 March 2006 / Accepted: 11 February 2007 / Published online: 13 September 2007
© International Association for Mathematical Geology 2007

Abstract Methods reported in the literature for rock fracture simulations include approaches based on stochastic geometry, multiple-point statistics and a combination of geostatistics for fracture density and object-based modelling for fracture geometries. The advantages and disadvantages of each of these approaches are discussed with examples. By way of review, the authors begin with the geostatistical indicator simulation method, based on the truncated–Gaussian algorithm; this is followed by multiple-point statistical simulation and then the stochastic geometry approach, which is based on marked point process simulation. A new approach, based on pluri-Gaussian structural simulation, is then introduced. The new approach incorporates in the simulation the spatial correlation between different sets of fractures, which in general, is very difficult, if not impossible, to accomplish in the three methods reviewed. Each simulation method is summarised together with detailed simulation procedures for each. A published two-dimensional fracture dataset is used as a means of assessing the performance of each simulation method and of demonstrating the concepts discussed in the text.

Keywords Stochastic rock fracture simulation · Indicator simulation · Marked point processes · Multiple-point statistics · PluriGaussian simulation

P.A. Dowd (✉)

Faculty of Engineering, Computer and Mathematical Sciences, University of Adelaide, Adelaide,
Australia
e-mail: peter.dowd@adelaide.edu.au

C. Xu · R.J. Fowell

School of Civil and Environmental Engineering, University of Adelaide, Adelaide, Australia

K.V. Mardia

Department of Statistics, University of Leeds, Leeds LS2 9JT, UK

Introduction

The stochastic simulation of rock fractures provides a powerful means of investigating rock mass properties related to fractures and fracture networks. The applications include rock engineering (Einstein and Stephansson 2000; Einstein 2003), water resources engineering (Long and Witherspoon 1985), petroleum engineering (Odling 1992) and hazardous waste disposal programmes (Dershowitz et al. 1999; Outters 2003). In general, in these applications, extensive sampling is difficult or expensive and the data available at the time of decision-making are scarce. For these reasons, the only feasible approach is via stochastic models based on the limited available data.

The intuitive approach to the problem is via stochastic geometry and thus Boolean models (or object-based models) and their extension, marked point process models, are common in the literature—see, for example, Chilès and Delfiner (1999), Lantéjoul (2002), Kulatilake et al. (1993), Lee et al. (1990), Stoyan et al. (1995). Approaches using geostatistics can also be found but, in general, they are applied within the context of Poisson modelling (Gringarten 1997; Long and Billaux 1987; Billaux et al. 1989; Wen and Sinding-Larsen 1997) where geostatistics plays only a small part in the total simulation process (usually limited to the modelling of fracture density). To the authors' knowledge, fracture simulation using only standard two-point geostatistics is very recent (Tomsett 2005). Multiple-point statistics (Bayesian modelling) has also been attempted (Guardiano and Srivastava 1993), but the scope of the study was limited. A Markov Chain Monte Carlo (MCMC) approach is currently being developed and the early results are very encouraging (Mardia et al. 2007).

In this paper, we compare the performances of the three major approaches, stochastic geometry, multiple-point statistics and the combination of geostatistics and object-based models. Sequential indicator simulation using multiple-point statistics is done within a Bayesian framework using a training image. The stochastic geometry approach is investigated in the form of marked point processes. The third approach is in the form of a proposed method based on the pluriGaussian algorithm, which provides a means of accounting for the spatial correlation between different subsets of fractures during the simulation. For completeness, sequential indicator simulation using the truncated Gaussian algorithm is also included as it provides the foundation for the pluriGaussian method and demonstrates why multiple-point statistics are necessary to simulate complex structures such as fractures.

Although all methodologies described in this paper are readily applicable in 3D, we have chosen to use a published two-dimensional dataset to demonstrate the concepts. The dataset comprises mapped fractures from the Yucca Mountain nuclear waste disposal project collected and reported by Barton and Larson (1985). It was used extensively by Lee et al. (1990) for their hierarchical modelling in which fractures are divided into subsets that are then modelled and simulated sequentially (with imposed hierarchical relations) to mimic different stages of fracture formation. Figure 1a shows the original fracture map and the digitized fracture traces are shown in Fig. 1b. Figure 1c shows the pixelated fracture traces, which can be viewed as an indicator representation of the dataset. A black pixel at x corresponds to $I(x) = 1$, meaning at least one fracture trace passes through the pixel centered on x . Depending on the accuracy required, different resolutions can be used to pixelate the fractures.

In our example, the resolution used is 200 pixels \times 200 pixels. If the centroids of the fractures are used to represent the locations of fractures, the point dataset shown in Fig. 1d is obtained. The original geographical ranges covered (Fig. 1a) are [0, 27] for the horizontal axis and [0, 21] for the vertical axis. In Figs. 1b–d, these ranges are reduced to [1.5, 25.5] and [2.5, 20], respectively. These ranges also apply to Fig. 2b, Figs. 3(a–d), Fig. 6(a), Figs. 8(a–b) and Fig. 9(a) and to all non-parametric density models $\lambda(x)$ shown in Table 1. Labels of the axes for these figures have been removed for more effective usage of the space. Note that this is an exhaustive dataset and the experimental model describing the fracture pattern can be directly estimated. Such a dataset makes for a more rigorous assessment of the performances of different simulation methods because model uncertainty can be kept to a minimum.

Truncated Gaussian Indicator Simulation

The indicator function for Fig. 1c is defined as

$$I(x) = \begin{cases} 1 & \text{if } x \in F \\ 0 & \text{otherwise} \end{cases} \tag{1}$$

where F is the random set of the pixelated fractures (black pixels in Fig. 1c). The image thus defined is binary and can be viewed as consisting of two complementary geological facies. The (unconditional) simulation can then be performed by the truncated Gaussian method (Galli et al. 1994). Three thresholds, $(-\infty, t^1, \infty)$, are required for the simulation, where $t^1 = G^{-1}(P_1)$ and P_1 is the proportion of pixels in Fig. 1c with $I(x) = 1$, which is 19.84%, and therefore, $t^1 = -0.8472$. The experimental variogram of $I(x)$ is plotted as black triangles in Fig. 2a. This variogram is used with least-squares fitting to derive the covariance model for the underlying Gaussian field, $Y(x)$, which is simulated and to which the thresholds are applied to simulate the indicators. The relationship between the spatial covariance, $C(h)$, of $I(x)$ and the spatial covariance, $\sigma(h)$, of $Y(x)$, is (Galli et al. 1994).

$$C(h) = \frac{1}{2\pi\sqrt{1 - \sigma^2(h)}} \int_{-\infty}^{t^1} \int_{-\infty}^{t^1} \exp\left[-\frac{u^2 + v^2 - 2\sigma(h)uv}{2(1 - \sigma^2(h))}\right] du dv. \tag{2}$$

Spherical models are assumed for both spatial covariances and the covariance model for $Y(x)$ derived from (2) has a range, $a = 4$ m. The theoretical variogram of $I(x)$, based on the derived covariance model, is shown as the solid line in Fig. 2a.

Once the Gaussian field, $Y(x)$, is simulated (e.g., using sequential simulation, Deutsch and Journel 1992), it is truncated to derive the realisation of $I(x)$ by applying the rule

$$\hat{I}(x) = \begin{cases} 1 & \text{if } -\infty < \hat{Y}(x) \leq -0.8472 \\ 0 & \text{otherwise.} \end{cases} \tag{3}$$

For one such realisation, the variogram of the simulated indicators is plotted using solid circles in Fig. 2a and the simulation is shown in Fig. 2b, in which the proportion of black pixels is 20.6%. Although the variogram model of $I(x)$ is reproduced

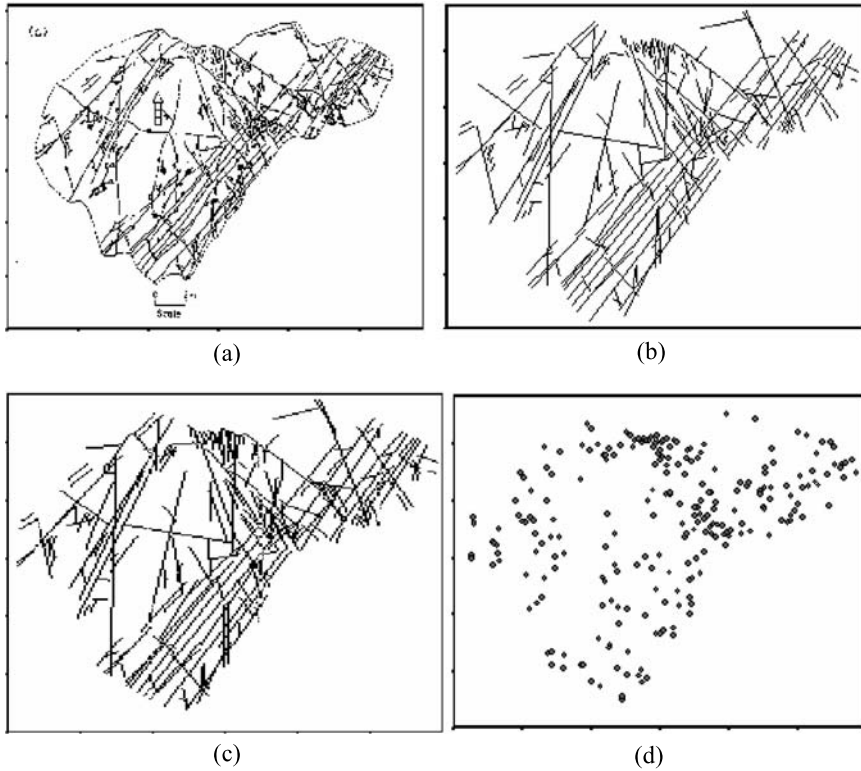


Fig. 1 a Fracture traces; b Digitised fractures; c Pixelated fractures; d Point data set

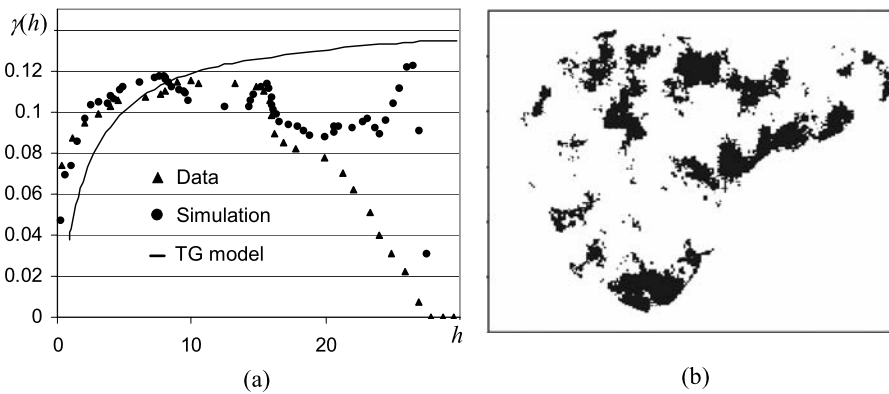


Fig. 2 a Variogram modelling; b A simulation of $I(x)$

reasonably well, the simulated image differs significantly in many respects to the original image shown in Fig. 1. This confirms previously reported observations that matching first and higher order properties of a random field does not necessarily re-

sult in the identical random process (Baddeley and Silverman 1984). In this case, the properties used for the simulation include the first order property of proportion and the second order property of the variogram.

Indicator Simulation Using Multiple-Point Statistics

The use of only first and second order properties is clearly inadequate for simulating the complex structures of the example fracture set. Using higher order statistics should improve the simulation although reconstruction of all the stochastic properties of the random field cannot be guaranteed (Baddeley and Silverman 1984). Inference of higher order spatial statistical models is difficult as they are based on spatial configurations rather than the simple pairwise distances and orientations used in the traditional forms of geostatistics. One approach is to use conditional probability for a particular configuration to infer experimentally the spatial model to describe the random field (Guardiano and Srivastava 1993; Strebelle 2002). For an indicator variable, such as $I(x)$ defined above, this conditional probability is equivalent to the conditional expectation of the configuration.

The conditional probability that $I(x) = 1$, given n data events $I(x_i) = 0$ or 1 , $i = 1, 2, \dots, n$, can be expressed as the sum of the $(2^n + 1)$ terms as follows

$$\begin{aligned} & \text{Prob}\{I(x) = 1 \mid I(x_i), i = 1, 2, \dots, n\} \\ &= \lambda_0 + \sum_{i=1}^n \lambda_i^{(1)} I(x_i) + \sum_{i=1}^n \sum_{j>i}^n \lambda_{ij}^{(2)} I(x_i) I(x_j) \\ &+ \sum_{i=1}^n \sum_{j>i}^n \sum_{k>j}^n \lambda_{ijk}^{(3)} I(x_i) I(x_j) I(x_k) + \dots + \lambda_{ijkl\dots}^{(n)} \prod_{m=1}^n I(x_m) \end{aligned} \tag{4}$$

where $\lambda_{\dots}^{(\dots)}$ are $2^n + 1$ coefficients obtained by an extended simple kriging system; see Guardiano and Srivastava (1993) for more details. The first $(n + 1)$ terms can be solved by kriging (unbiasedness condition and two-point statistics) and the other terms describe multiple point statistical characteristics of order 3 to n . In practice, inference of all the models of different orders to describe fully this conditional probability is almost impossible, especially when n is large. However, a reduced set of this conditional probability can be used instead. This reduced set amounts to choosing the situation for which $I(x_i) = 1$, $i = 1, 2, \dots, n$, one of the possible 2^n joint realisations of the n events. An experimental dataset (one realisation of the random field) can then be used to evaluate this conditional probability by using the Bayesian conditional probability postulate

$$\begin{aligned} & \text{Prob}\{I(x) = 1 \mid I(x_i) = 1, i = 1, 2, \dots, n\} \\ &= \frac{\text{Prob}\{I(x) = 1, I(x_i) = 1 (i = 1, 2, \dots, n)\}}{\text{Prob}\{I(x_i) = 1 (i = 1, 2, \dots, n)\}} \end{aligned} \tag{5}$$

which, for an indicator variable, is equal to the conditional expectation of $I(x)$ given $I(x_i) = 1$, $i = 1, 2, \dots, n$. Once this conditional probability is inferred, $I(x)$ can be

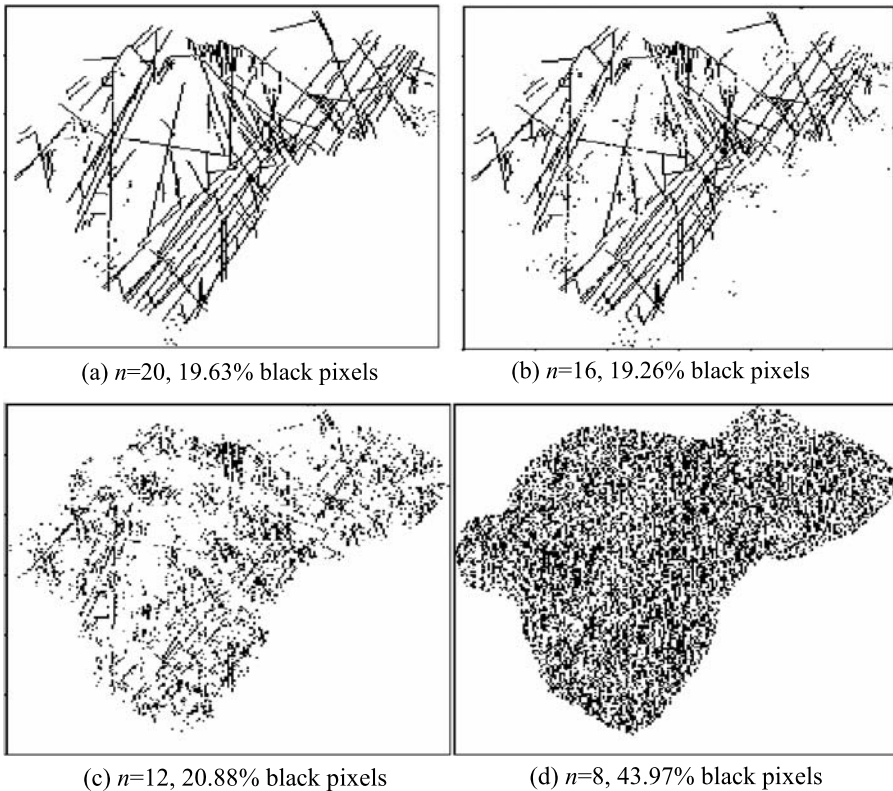


Fig. 3 Multiple-point statistical simulations

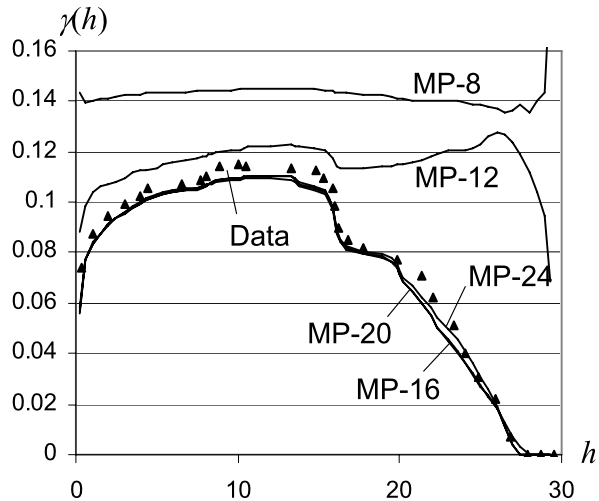
simulated by Monte Carlo sampling. The inference is usually based on one or more realisations of the random variable, which are referred to as training images. These training images may be datasets or they may be postulated on the basis of expert knowledge.

The four steps required for the sequential simulation of $I(x)$ using the conditional probability approach (Guardiano and Srivastava 1993; Strebelle 2002) are:

- Define a random path through the simulation grid.
- At each grid node, x , retain the nearest n indicator data, $I(x_i)$, $i = 1, 2, \dots, n$ (conditioning data and previously simulated indicators). Scan the training image for all $(n + 1)$ -tuples that replicate the x plus n data configuration and evaluate $\text{Prob}\{I(x_i) = 1 \ (i = 1, 2, \dots, n)\}$ and $\text{Prob}\{I(x) = 1, I(x_i) = 1 \ (i = 1, 2, \dots, n)\}$, and hence obtain the conditional probability $\text{Prob}\{.\}$ given in (5).
- Simulate $I(x)$ based on $\text{Prob}\{.\}$ using Monte Carlo sampling and then add $I(x)$ as a known datum event.
- Move to the next grid node and repeat.

The choice of n is critical as it determines the complexity of the structures that can be adequately reproduced. Figures 3(a–d) show the simulation of the fracture

Fig. 4 Two-point variogram models for multiple-point statistical simulation



example using $n = 20, 16, 12$ and 8 , respectively. The figures clearly indicate that for $n \geq 20$ the simulation generates structures that are almost identical to the training images used to construct the probability models. For $n = 16$, the simulated image shows signs of fragmenting, which increases as n is further reduced until for $n = 8$, the simulation shows no resemblance to the original image. Note, however, that the proportion of black pixels does not change significantly from that of the training image until $n = 8$ when the proportion is more than doubled.

It is difficult to evaluate the quality of the multiple-point statistical simulations using the conditional expectation model in (4). We use here only the two-point variogram models as a simple verification that the second-order correlations are reproduced, and the results are given in Fig. 4. As expected, the reproduction of the variogram model is excellent for $n \geq 16$ whilst there are significant differences when $n \leq 12$.

These simulations demonstrate clearly the importance of n as a parameter in multiple-point statistical simulation and the need for a careful choice of its value, which depends on the complexity of the structures to be simulated. In the example given here, it can be reasonably concluded that values of $n \leq 12$ are inadequate to describe statistically the complexity of the structures.

The ability to model complex structures makes this simulation technique an attractive choice for rock fracture simulations. Another merit of the method is that it can easily be extended for applications in higher dimensions (≥ 3). The major drawback is the difficulty of inferring the probability models with the consequent need to (over) rely on training images. It is noted that Guardiano and Srivastava (1993) made some attempt to model partially the conditional expectation in (4).

Note that the indicator-based simulations described here are based on pixelated fracture patterns and the simulation output is also in pixels. For subsequent analyses, such as connectivity and flow assessment of the fracture network, geometric fractures (continuous lines in two dimensions or continuous surfaces in three dimensions) could be constructed from the pixelated image (a reverse pixelation process).

This process is fairly simple provided the fracture pattern is adequately simulated, such as that shown in Fig. 3(a).

Simulation Using Marked Point Process Models

In the context of marked point processes, in two dimensions, the simulation of fractures is equivalent to the simulation of a line segment process (a special case of a fibre process) and in three dimensions, it is equivalent to the simulation of a surface (polygon) process (Stoyan et al. 1995; Dershowitz and Einstein 1988). In this approach, the spatial location of each fracture, f , in the fracture set F (considered as a realisation of a stochastic geometry model \mathbf{F}) is represented by a point x in space where x usually coincides with a featured point in f , such as the centroid of a fracture plane (or line). Properties associated with f (e.g., sizes, orientations) are then represented using marks, m , assigned to point x . The collection $\{x\}$ then forms a point pattern P considered as a realisation from a point process model, \wp . The collection $\{x, m\}$ is considered to be a marked point pattern, M , which is realised from a marked point process model, \mathbf{M} , related to \wp . If \mathbf{M} can be inferred for an application, the marked point pattern can then be simulated, and hence a simulated fracture set can be generated.

It is common practice to classify rock fractures into sub-sets defined by ranges of orientations, which in turn are defined by geological and/or geomechanical considerations (Lee et al. 1990; Kulatilake et al. 1993). Lee et al. (1990) classified the example dataset into two sub-sets and performed the simulation using a complex hierarchical model. In our view, a better reconstruction (i.e., better reproduction of the original structures) can be achieved by using more sub-sets together with simple Boolean object simulation, provided each individual fracture sub-set can be satisfactorily modelled (refer to results below).

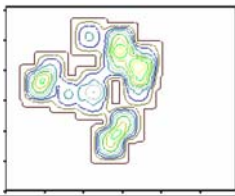
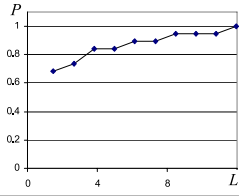
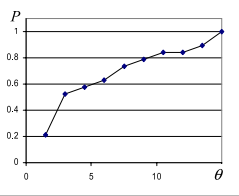
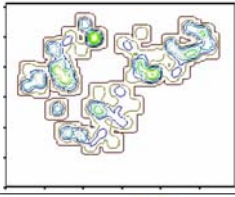
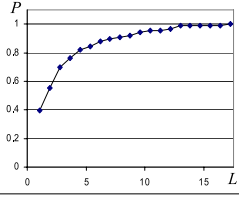
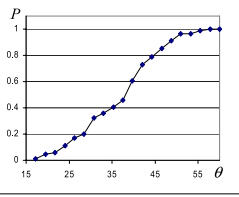
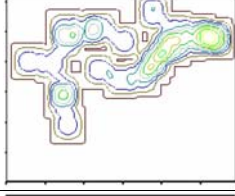
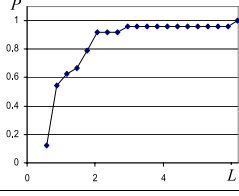
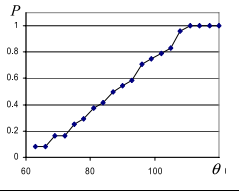
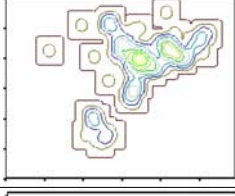
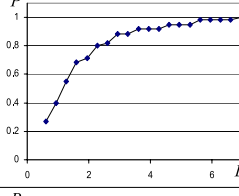
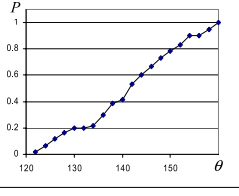
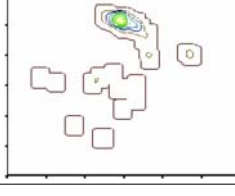
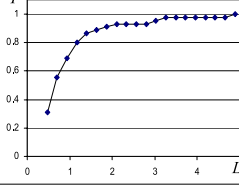
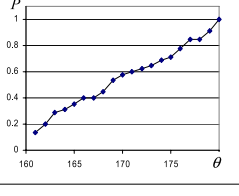
Figure 5 shows the rose diagram of the doubled azimuth angles of the fractures in the example dataset. The data have been classified into five sub-sets according to fracture orientation and each sub-set is modelled separately. The combination of all individually simulated fracture sub-sets forms the final simulated fracture pattern.

The method comprises three steps:

- For each fracture sub-set, simulate the fracture locations from the corresponding point intensity model $\lambda(x)$, thus generating a realisation of the point process model for each sub-set.
- For each point of the point realisation, simulate the marks, i.e., fracture properties (length and orientation for this example) from their respective probability distribution function (PDF) using Monte Carlo sampling.
- Combine the simulations of all sub-sets to obtain the complete simulation (considered as a realisation of the underlying stochastic geometry model \mathbf{F}).

A point density model, $\lambda(x)$, and a PDF for each mark of each sub-set are required for the simulation. For the example used, these models are given in Table 1 where $\lambda(x)$ is estimated by the kernel estimation method using the Epanechnikov kernel (Cressie 1993; Xu et al. 2007). Note that both non-parametric and parametric models can be

Table 1 Models used for the marked point process simulation

	$\lambda(x)$	PDF(Length)	PDF(Azimuth angle)
Set 1			
Set 2			
Set 3			
Set 4			
Set 5			

established and used although only non-parametric models are used in this example. The use of non-parametric models estimated directly from the dataset ensures more accurate point process models for the simulations and the performances of the simulation method as a whole can be more easily assessed (without the complication of model uncertainty).

Figure 6(a) shows a fracture pattern generated by this simulation technique. As a quality check on the simulation, the inter-fracture distance function $H(h)$ and the analogous K -function, $K(h)$, defined for a line segment process from the simulation output and the data are compared. To calculate $H(h)$ and $K(h)$, each fracture is represented by a random point on the fracture and hence an associated point pattern is created for each fracture realisation. Point process statistics for the converted point

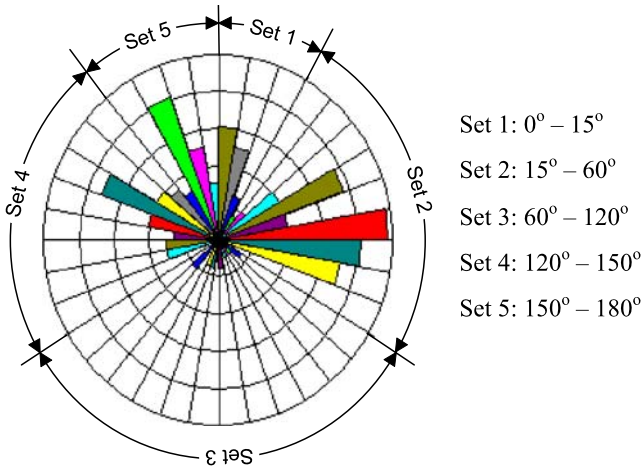
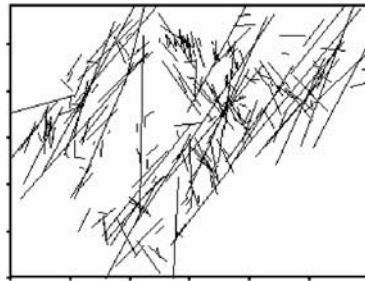
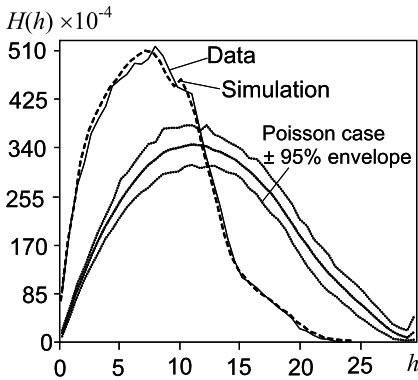


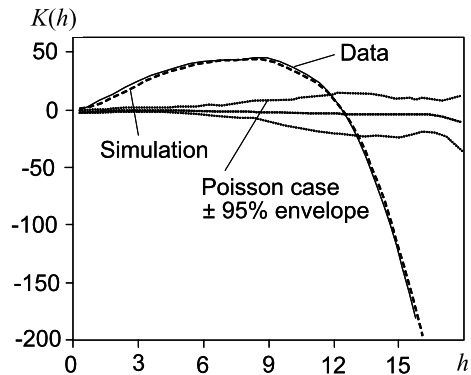
Fig. 5 Rose diagram of the doubled azimuth angles of the example dataset



(a) A simulated fracture pattern



(b) Inter-line distance function



(c) *K*-function of line process

Fig. 6 A simulated fracture pattern and statistical comparison with the dataset

pattern are then used to characterize the properties of the underlying line segment process (Parker and Cowan 1976; Stoyan et al. 1995). $H(h)$ and $K(h)$ are then calculated, respectively, as the inter-event distance and the K -function of point process statistics (Diggle 2003). $H(h)$ therefore represents, loosely speaking, the statistics of average spacing between fractures and $K(h)$ represents their spatial correlations. The functions for the simulation output and the dataset are given in Figs. 6(b) and (c). Clearly, these statistics are very well reproduced in the simulated fractures. The functions for spatially independent cases (i.e., Poisson line processes) are also plotted with their 95% confidence envelopes based on the Monte Carlo test method (Diggle 2003). As expected, there are considerable differences between the functions, confirming that the modelled line segment process is non-homogeneous.

The marked point process is directly applicable to three-dimensional cases and there is no additional complexity over the two-dimensional case. The marks of the points are replaced by those describing the three-dimensional geometries of the fracture planes (Poisson polygons). The annealing technique proposed by Xu et al. (2007) can be used to include auto-correlations and cross-correlations between marks in the simulations. If correlations between point locations of different sub-sets are relevant to the application, then either the hierarchical approach proposed in Lee et al. (1990) or the pluriGaussian approach, described below, can be used.

Rock Fracture Simulation by the PluriGaussian Method

In the marked point process it is very difficult to incorporate spatial correlations among fracture sets. A relatively straightforward way of doing so is provided by geostatistical pluriGaussian method. PluriGaussian simulations (Le Loc'h and Galli 1996; Dowd et al. 2003) significantly extend the capabilities of the truncated Gaussian method for the simulation of complicated structures (Armstrong and Dowd 1994; Xu et al. 2006). Here we use the method to simulate the locations of fractures. The method, however, can also be applied directly to a pixelated fracture indicator field.

For m sub-sets ($m = 5$ in the example) of fractures, we define m indicator variables as follows

$$I_k(x) = \begin{cases} 1 & \text{if } x \in F_k \\ 0 & \text{otherwise} \end{cases} \quad k = 1, \dots, m \quad (6)$$

where F_k is the set of points representing the locations (e.g., centroids of fractures) of the k th sub-set fractures (see Fig. 1d). If a complete mutual contact relationship is assumed between the sub-sets, $n = (m - 1)$ ($n = 4$ in the example) simulated Gaussian fields can be truncated to obtain the simulated locations of the fractures. The spatial auto-correlations of the fracture sets and the cross-correlations between the sub-sets will be honoured indirectly by the n simulated correlated Gaussian fields.

The truncation of n Gaussian variables for m distinct partitions (representing m defined indicator variables) in the combined n -dimensional Gaussian space, requires three thresholds (hence, two partitions) for each Gaussian if the full contact relationship is assumed. The thresholds are related directly to the proportions of each sub-set

Table 2 Proportions, thresholds and Gaussian models for the simulation

	Set 1	Set 2	Set 3	Set 4	Set 5
P_k (data)	0.0802	0.3755	0.1013	0.2531	0.1899
P_k (simulation)	0.0652	0.3728	0.1009	0.2682	0.1930
P_k (after erosion)	0.0729	0.3320	0.1296	0.2632	0.2024

	t^1	t^2	t^3	Model
Gaussian 1	$-\infty$	-1.404	$+\infty$	Exponential with $a = 1.1$
Gaussian 2	$-\infty$	-0.228	$+\infty$	Exponential with $a = 2.0$
Gaussian 3	$-\infty$	-0.888	$+\infty$	Exponential with $a = 1.5$
Gaussian 4	$-\infty$	0.18	$+\infty$	Exponential with $a = 1.4$

of indicators. The proportion of the combined Gaussian space ($\equiv 1$) comprised by the k th partition of the space, representing the k th sub-set, is (Xu et al. 2006)

$$P_k = \int_{t_1^k}^{t_1^{k+1}} \int_{t_2^k}^{t_2^{k+1}} \cdots \int_{t_n^k}^{t_n^{k+1}} f(z_1, z_2, \dots, z_n) dz_1 dz_2 \cdots dz_n \tag{7}$$

where $f(\cdot)$ is the joint density of n Gaussian variables, and $t_j^k \rightarrow t_j^{k+1}$ is the threshold applied to the j th Gaussian to form the k th partition. $P_k, k = 1, \dots, m$, can be estimated from the data and thus so can all the thresholds. The auto- and cross-covariances between pairs of indicators are directly related to the auto- and cross-covariances between the Gaussian variables. For example, the covariance between the i th and the j th indicators can be expressed using the covariance model of the joint $2n$ -dimensional Gaussian distributions

$$C_{ij}(h) = \int_{t_1^i}^{t_1^{i+1}} \int_{t_2^i}^{t_2^{i+1}} \cdots \int_{t_n^i}^{t_n^{i+1}} \int_{t_1^j}^{t_1^{j+1}} \int_{t_2^j}^{t_2^{j+1}} \cdots \int_{t_n^j}^{t_n^{j+1}} f_{\Sigma}(y_1, y_2, \dots, y_n, z_1, z_2, \dots, z_n) dy_1 dy_2 \cdots dy_n dz_1 dz_2 \cdots dz_n \tag{8}$$

where Σ , the covariance matrix for the $2n$ Gaussian variables, is defined by the covariance models of the Gaussian variables separated by distance h , and $f_{\Sigma}(\cdot)$ is the joint $2n$ -variate Gaussian density defined by Σ . See Armstrong et al. (2003, p. 60) for an example of the form of Σ for the two Gaussian cases. Based on the established relations, the experimental $C_{ij}(h)$ can then be used to estimate the Gaussian covariance models required for simulating the n Gaussian fields (cf. Dowd et al. 2003; Xu et al. 2006, for detailed implementations).

For the example used in this paper, the thresholds required for the truncations are listed in Table 2. The auto- and cross-variograms of the indicators used in deriving the covariance models (also listed in Table 2) for the four Gaussians used in the

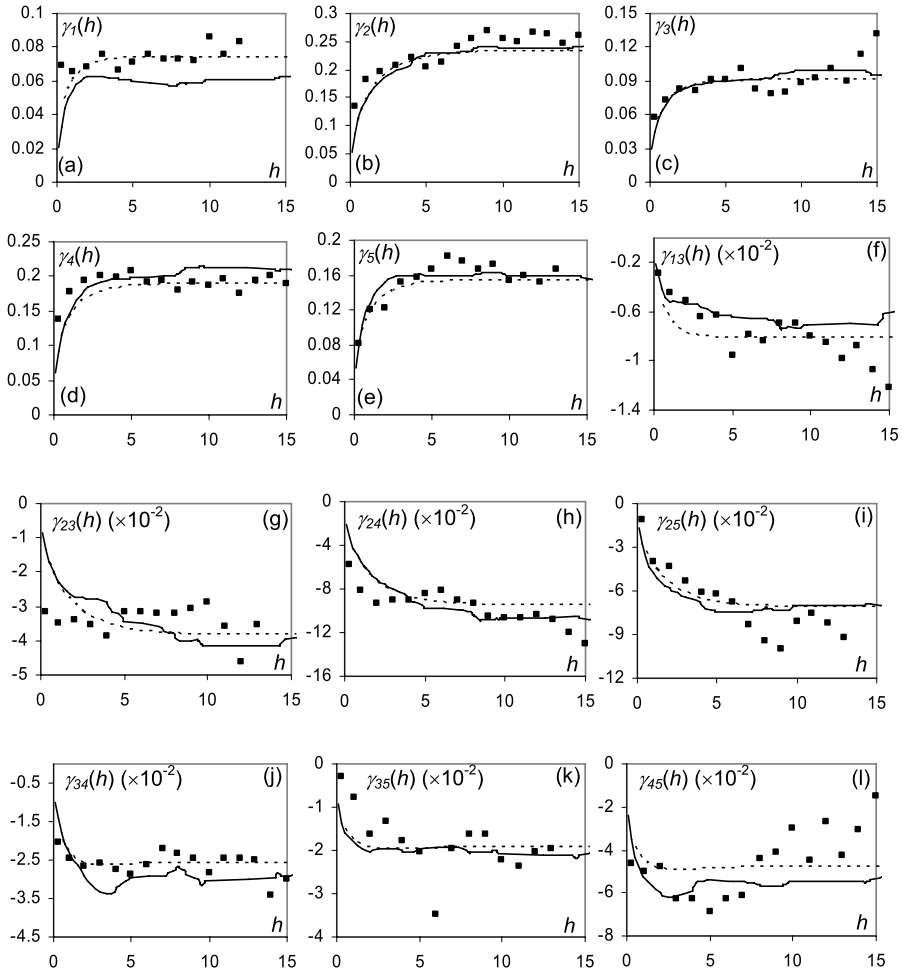


Fig. 7 Auto- and cross-variograms used in the pluriGaussian simulation

simulation are given in Fig. 7. Note that, for convenience, auto- and cross-variograms are used instead of auto- and cross-covariances. In Fig. 7, black squares represent experimental variograms, solid lines are the variograms calculated from the simulated data and the broken lines are the theoretical models calculated from the Gaussian models. The simulation was done on a 200×200 grid.

A few observations can be made of Fig. 7. First, all correlation structures are satisfactorily reproduced, especially for the auto-correlations. Secondly, as the magnitudes of the nugget variances and sill values of the variograms are, in general, significantly greater than those of the cross-variograms, they have a much greater influence on the covariance models of the four Gaussian variables. Finally, not all cross-variograms are used in the simulation; extremely noisy experimental variograms were excluded from the modelling process so as to minimise distorting effects.

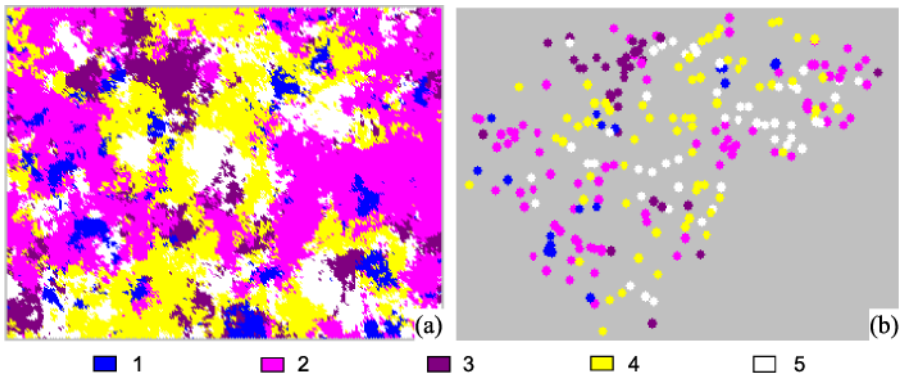


Fig. 8 PluriGaussian simulations of fracture locations before and after erosions

The simulation comprises the combined set $\bigcup_{k=1}^m F_k$ (i.e., $\sum_{k=1}^m P_k = 1$), which is only a subset of the whole problem. The simulated image at this stage contains only the five indicator values, as shown in Fig. 8(a). To simulate the final fracture locations, this image is “eroded”. We propose here the use of a two step erosion process:

- Geostatistical erosion. Define a masking variable, $N(x)$, using a grid size much larger than the original simulation grid (200×200), which in the example results in a masking grid of 16×12 cells. $N(x)$ is defined as the number of fractures inside the larger grid cell centred at x . $N(x)$ is then modelled from the known, or conditioning, dataset. The model is then used to perform an unconditional simulation of $N(x)$ using any geostatistical simulation method (sequential Gaussian was used in the example). Finally, the simulated $N(x)$ is applied to $\bigcup_{k=1}^m I_k$ (Fig. 8(a)) and all I_k , $k = 1, \dots, m$ indicators within the larger grid cell for which $N(x) = 0$ are removed (eroded). The size for the large grid is normally chosen such that the proportion of larger grid cells having at least one fracture is around 50%. Such a choice is optimal in terms of retaining the spatial correlations of fracture locations.
- Monte Carlo erosion: For each large grid cell having at least one fracture and centred at x , retain $N(x)$ fractures chosen at random Monte Carlo sampling is used in this step.

The fracture locations remaining after the erosions comprise the final simulated fracture locations. For the example dataset, the simulation result is given in Fig. 8(b). These locations are then used with the PDF of fracture length and orientation shown in Table 2 to simulate the final fracture pattern. One such simulated image is shown in Fig. 9(a). The quality of the simulation is again tested by the inter-fracture distance function and the line process K -function, which are shown in Figs. 9(b) and (c). The inter-fracture distance function was satisfactorily reproduced by the simulation but there are some differences in the line process K -function between the simulation and the data. The simulated image is also a poorer reconstruction of the original image compared with that achieved by the marked point process simulation. This exercise does, however, demonstrate the feasibility of using the pluriGaussian method for rock fracture simulations. The method, as proposed in the context of this application, is

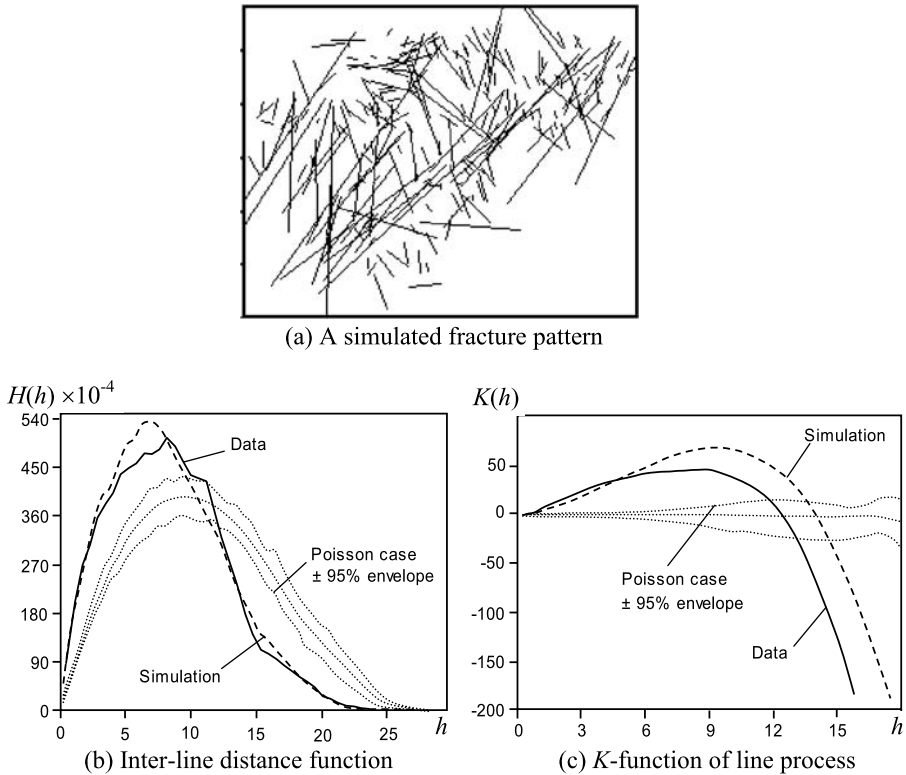


Fig. 9 PluriGaussian simulated fracture pattern and corresponding statistics

still at an early stage of development and further research is required to investigate the sensitivity of simulations to the grid size and to the erosion (thinning) process.

The pluriGaussian method described here can also be directly applied to three-dimensional applications without any modification. This simulation method introduces correlations between different point sets (sub-sets fracture locations), which in general is difficult to implement using only marked point process modelling.

Conclusions

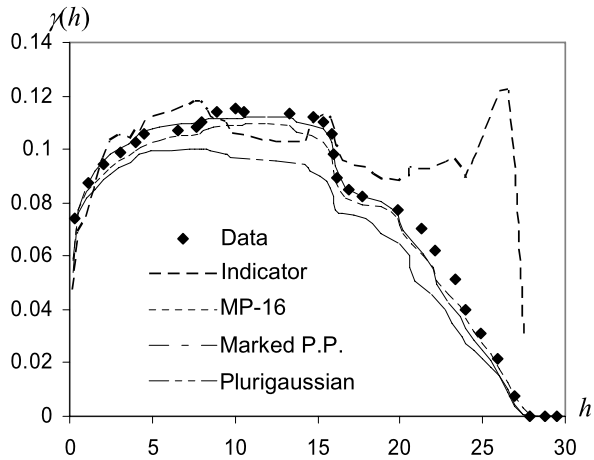
As a final remark on the comparison of the four simulation methods, the simulated images of Figs. 6(a) and 9(a) have been pixelated using the resolution of 200×200 pixels. The major statistical characteristics of the four simulations are compared with those of the dataset in Table 3 and Fig. 10.

The following conclusions can be drawn from this study:

- Two-point indicator-based geostatistical simulation is inadequate for the simulations of complex structures such as rock fractures.

Table 3 Proportion of black pixels in the simulations

	Data	Indicator simulation	Multiple-point statistics	Marked point process	PluriGaussian
Proportion of black pixels (%)	19.84	20.60	19.26	21.11	19.02

Fig. 10 Variograms of the simulations

- Rock fractures can be simulated satisfactorily by multiple-point statistical methods. Although the number of orders of statistics required for satisfactory simulation depends on the complexity of the fracture pattern, on the basis of examples, such as that reported here, it has been demonstrated the order must be at least 16 to obtain satisfactory results.
- The use of marked point processes for rock fracture simulation has been demonstrated again to be a relatively simple method that will generate very good results provided the fracture properties can be described accurately by marks. From comparisons with published simulations based on the same dataset, it has been found that the use of more, smaller sub-sets will, in general, produce better results than the use of fewer, larger sub-sets provided that all sub-sets can be satisfactorily modelled.
- The pluriGaussian method can also be used for rock fracture simulations. The method provides a means of introducing spatial correlations between different sub-sets of fractures, which may be difficult to achieve using methods such as marked point processes.

All the methods described can be readily applied to 3D fracture modelling and simulations without major modifications.

Acknowledgements The work reported in this paper was funded by EPSRC (Engineering and Physical Sciences Research Council) Research Grant Number GR/R94602/01.

References

- Armstrong M, Dowd PA (eds) (1994) Geostatistical simulations. In: Proceedings of the geostatistical simulation workshop, Fontainebleau, France, 27–28 May 1993. Kluwer Academic, London, p 268
- Armstrong M, Galli GA, Le Loc'h G, Geffroy F, Eschard R (2003) PluriGaussian simulations in geosciences. Springer, Berlin
- Baddeley AJ, Silverman BW (1984) A cautionary example on the use of second-order methods for analysing point patterns. *Biometrics* 40:1089–1094
- Barton CC, Larson E (1985) Fractal geometry of two-dimensional fractures networks at Yucca Mountain, Southwest Nevada. In: Stephanson O (ed) Proceedings of the international symposium on fundamentals of rock joints. Centek, Lulea, p 582
- Billaux D, Chiles JP, Hestir K, Long J (1989) Three-dimensional statistical modelling of a fractured rock mass—an example from the Fanay-Augères mine. *Int J Rock Mech Min Sci Geomech Abstr* 26(3/4):281–299
- Chilès J-P, Delfiner P (1999) Geostatistics: modeling spatial uncertainty. Wiley, New York, p 695
- Cressie NAC (1993) Statistics for spatial data—revised edition. Wiley, New York, p 928
- Dershowitz WS, Einstein HH (1988) Characterizing rock joint geometry with joint system models. *Rock Mech Rock Eng* 21:21–51
- Dershowitz B, Eiben T, Follin S, Andersson J (1999) Alternative models project—discrete fracture network modelling for performance assessment of Aberg. Technical report R-99-43, Svensk Kärnbränslehantering AB. www.skb.se
- Deutsch C, Journel AG (1992) Geostatistical software library and user's guide. Oxford University Press, Oxford
- Dowd PA, Pardo-Igúzquiza, Xu C (2003) Plurigaou: a computer program for simulating spatial facies using the truncated pluriGaussian method. *Comput Geosci* 29:123–141
- Diggle P (2003) Statistical analysis of spatial point patterns, 2nd edn. Edward Arnold, London, p 306
- Einstein HH, Stephansson O (2000) Fracture systems, fracture propagation and coalescence. In: Proceedings of the international conference on geotechnical & geological engineering, Melbourne, Australia. Technomic, Lancaster, pp 1348–1388
- Einstein HH (2003) Uncertainty in rock mechanics and rock engineering—then and now. In: Proceedings of ISRM 2003 conference—technology roadmap for rock mechanics. South Africa institute of mining and metallurgy symposium series S33, vol 1, pp 281–293
- Galli A, Beucher H, Le Loc'h G, Doligez B (1994) The pros and cons of the truncated Gaussian method. In: Armstrong M, Dowd PA (eds) Geostatistical simulations. Kluwer Academic, London, p 255
- Guardiano F, Srivastava RM (1993) Multivariate geostatistics: beyond bivariate moments. In: Soares A (ed) Geostatistics Troia 1. Kluwer Academic, Dordrecht, pp 133–144
- Gringarten E (1997) 3D geometric description of fractured reservoirs. In: Baafi EY, Schofield NA (eds) Geostatistics Wollongong '96, vol 1. Kluwer Academic, Dordrecht, pp 424–432
- Kulatilake PHSW, Wathugala DN, Stephansson O (1993) Joint network modelling with a validation exercise in Stripa Mine, Sweden. *Int J Rock Mech Min Sci* 30:503–526
- Lantéjoul C (2002) Geostatistical simulation, models and algorithms. Springer, Berlin
- Lee JS, Veneziano D, Einstein HH (1990) Hierarchical fracture trace model. In: Hustrulid W, Johnson GA (eds) Rock mechanics contributions and challenges. Proceedings of the 31th US rock mechanics symposium, Balkema, Rotterdam, p 1082
- Le Loc'h G, Galli A (1996) Truncated pluriGaussian method: theoretical and practical points of view. In: Baafi EY, Schofield NA (eds) Geostatistics Wollongong '96, vol 1. Kluwer Academic, Dordrecht, pp 211–222
- Long JCS, Witherspoon PA (1985) The relationship of the degree of interconnection to permeability in fracture networks. *J Geophys Res* 90(B4):3087–3098
- Long JCS, Billaux DM (1987) From field data to fracture network modelling: an example incorporating spatial structure. *Water Resour Res* 23(7):1201–1216
- Mardia KV, Walder AN, Xu C, Dowd PA, Fowell RJ, Kent JT (2007) A line finding assignment problem and rock fracture modelling MCMC implementation of rock fracture modelling. In: Upadhyay SK, Singh U, Dey DJ (eds) Bayesian statistics and its applications. Anamaya, New Delhi, pp 319–330, ISBN 10 81-88342-63-7; ISBN 13 978-81-88342-63-1
- Odling NE (1992) Permeability and simulation of natural fracture patterns. In: Larsen RM, Brekke H, Larsen BT, Talleres E (eds) Structural and tectonic modelling and its application to petroleum geology. Norwegian Petroleum Society special publication 1. Elsevier, New York, p 549

- Outters N (2003) A generic study of discrete fracture network transport properties using FracMan/MANFIC. Technical report R-03-13, Svensk Kärnbränslehantering AB. www.skb.se
- Parker P, Cowan R (1976) Some properties of line segment processes. *J Appl Probab* 13:96–107
- Stoyan D, Kendall W, Mecke J (1995) *Stochastic geometry and its applications*, 2nd edn. Wiley, Chichester
- Strebelle S (2002) Conditional simulation of complex geological structures using multiple-point statistics. *Math Geol* 34:1–21
- Tomsett A (2005) Geostatistical investigation of fractures within the crystalline rocks of Stripa Mine, Sweden. MSc thesis, Department of Mining and Mineral Engineering, The University of Leeds
- Wen R, Sinding-Larsen R (1997) Stochastic modelling and simulation of small faults by marked point processes and kriging. In: Baafi EY, Schofield NA (eds) *Geostatistics Wollongong '96*, vol 1. Kluwer Academic, Dordrecht, p 643
- Xu C, Dowd PA, Mardia KV, Fowell RJ (2006) PGSim: a flexible true pluriGaussian code for simulations of geological facies. *Comput Geosci* 32:1629–1645
- Xu C, Dowd PA, Mardia KV, Fowell RJ, Taylor CC (2007) Simulating correlated marked point processes. *J Appl Stat* 34(8) (in press)